

Supporting Information

Redox-active Polynaphthalimides as Versatile Electrode Materials for High Voltage, High-Rate and Long Cycle-Life Organic Li-ion Batteries

Febri Baskoro^{a,†}, Andre Lammiduk Lubis^{a,†}, Hui Qi Wong^{a,b,c}, Guey-Sheng Liou^{d,*}, Hung-Ju Yen^{a,*}

^a Institute of Chemistry, Academia Sinica, Taipei, Taiwan

^b Sustainable Chemical Science and Technology Program, Taiwan International Graduate Program, Academia Sinica and National Taiwan University, Taipei, Taiwan

^c Department of Chemical Engineering, National Taiwan University, Taipei, Taiwan

^d Institute of Polymer Science and Engineering, National Taiwan University, Taipei, Taiwan

E-mail: gслиou@ntu.edu.tw (G.-S. Liou); hjyen@gate.sinica.edu.tw (H.-J. Yen)

Supplementary Text

Supplementary Text 1- Electrode preparations and electrochemical measurements

The electrode used in this study were prepared using slurry method. In brief, the LiB cathode was prepared by mixing the active material (40 wt%), conductive carbon of super P (50 wt%), and PVDF (10 wt%). While, the anode is prepared by mixing 20% with Super P as conductive carbon (70%), and PVDF (10%). Both mixtures were then dissolved in *N*-methyl-2-pyrrolidone (NMP) forming a homogeneous slurry. The slurry was spread onto Copper foil (Cathode) or Aluminum foil (Anode) by using a doctor blade with the clearance of 100 μm . The slurry were then dried on the hot plate at 60 °C for 12 hours, and continued in the vacuum oven under 80 °C for another 8 hours. The electrodes were cut into 12-mm disks, then transferred into the glovebox for cell assembling process. The average mass loading of 0.62, 0.56, and 0.46 mg cm⁻² was obtained for **PNI-1**, **PNI-2**, and **PNI-3** cathodes, respectively. While, the mass loading of **PNI-1**, **PNI-2**, and **PNI-3** anodes was found around 0.78, 0.61, and 0.70 mg cm⁻². In addition, the binder free cathode was prepared using the same method with ratio of active material (40 wt%) and Super P as the conductive carbon (60 wt%), resulting mass loading of 0.58 and 0.60 mg cm⁻² for binder free **PNI-1** and **PNI-2**, respectively.

Finally, the coin cells of CR2032-type were assembled in a high-purity argon-filled glovebox ($\text{H}_2\text{O} < 0.5 \text{ ppm}$, and $\text{O}_2 < 0.5 \text{ ppm}$). Lithium foil with diameter of 12 mm used as counter electrode, Celgard 2325 as the separator, and 40 μL of 1 M LiPF₆ in a 1:1 (v/v) of ethylene carbonate/diethyl carbonate (EC/DEC) solution as electrolyte.

For electrochemical tests, the galvanostatic charge-discharge measurements were performed on a battery tester station (AcuTech Systems Co. Ltd) at voltage 1.5 – 4.5 V (vs. Li⁺/Li) for cathode and 0.02 – 3.0 V for anode. Cyclic Voltammetry (CV) measurements was performed using an electrochemical analyzer (MultiPalmSens4, PalmSens BV) at the same potential window with scan rate of 0.1 mV s⁻¹. The electrochemical impedance spectroscopy (EIS) analysis were conducted before and after battery cycle using CHI electrochemical

workstation model 760e, CH Instruments, Inc., with frequency range between 10 mHz to 1 MHz and alternating current (AC) voltage signal of 10 mV. The galvanostatic intermittent titration technique (GITT) has been carried out to probe the ion diffusion of PNIs system. The GITT measurement was performed using Squitstat potentiostats, Admiral Instrument by alternating current density of 50 mA g⁻¹ for 20 min with a rest interval of 10 min. Prior the GITT measurement, fresh coin cells were fully charged under 50 mA g⁻¹ and allowed to rest for up to 10 hours. The diffusion coefficient was then calculated by the following formula:

$$D = \frac{4}{\pi\tau} \left(\frac{m_B V_M}{M_B S} \right)^2 \left(\frac{\Delta E_s}{\Delta E_t} \right)^2$$

where D is diffusion coefficient (cm² s⁻¹), τ is the current pulse (s), m_B is the mass of the host material in the electrode (g), V_M is the molar volume of the material (cm³ mol⁻¹), M_B is the molecular weight of the host material (g mol⁻¹), and S is the contact area of the electrolyte and electrode interface (cm²). ΔE_s and ΔE_t are the voltage responses over the relaxation and current pulse, respectively.

Supplementary Text 2- Diffusion coefficient calculation based on EIS data

Electrochemical impedance spectroscopy (EIS) is a powerful tool to probe the electrochemical phenomena that occur in the complex electrochemical systems such as battery cells.¹ In general, the Nyquist plot of EIS spectra present electrochemical process in the three different frequency regions. First, the conduction across electrolyte, separator, and wires was reflected in the high frequency area.² Furthermore, the mid frequency is the region represents the charge transfer and kinetic reactions,^{3, 4} while the low frequency region is typically with slope of 45°, represents the diffusion limited region in the solid phase and is typically characterized by the Warburg impedance.⁵ Additionally, the Warburg impedance can be defined by :

$$\begin{aligned} Z' &= \sigma/\omega^{\frac{1}{2}} - j\sigma/\omega^{\frac{1}{2}} \\ |Z''| &= \sqrt{2}\sigma/\omega^{\frac{1}{2}} \end{aligned}$$

where Z' and Z'' are real and imaginary impedance, respectively. While, ω is the angular frequency and σ is the Warburg coefficient. Warburg coefficient (σ) can be determined by the slope of Warburg plot (Z' vs $1/\omega^{\frac{1}{2}}$). In Li ion battery, the relationship of Warburg coefficient (σ) and the diffusion coefficient (D) is given by :

$$\sigma = \frac{RT}{n^2 F^2 A \sqrt{2}} \left(\frac{1}{D_{Li}^{1/2} C_{Li}} \right)$$

where R is ideal gas constant, T is absolute temperature, n is the number of electron transferred, F is Faraday's constant, A is the area of the electrode, D_{Li} and C_{Li} are the diffusion coefficient and concentration of Li⁺, respectively.⁶

Supplementary Text 3- Sweep rate voltammetry for charge-storage characteristic

The sweep rate voltammetry is one of powerful technique that could to probe a consecutive electrochemical reactions which occurs in the electrodes. In general, the total charge in a CV curve can be classified into three components: (a) the faradaic contribution from the Li⁺ ion diffusion process; (b) the faradaic contribution from the charge-transfer process with surface atoms, referred to as pseudocapacitance; (c) the non-faradaic contribution from the

double layer effect.^{7,8} Moreover, the contribution of both types capacitive effects, such as pseudocapacitance and double layer effect, can be substantial due to the increasing surface area of the electrode.⁷ These faradaic contribution from diffusion-control and surface-control (capacitive effects) process can be characterized using CV data at various scan rates and expressed by the following formula:

$$i = av^b$$

where i is current response to the scan rate v , while a and b are constants. The b value can be obtained from the slope of $\log i$ vs $\log v$, see Fig. S15a-c. In addition, if the b value close to 0.5 would indicate half-infinite linear diffusion controlled process, meanwhile b value close to 1 indicates the current is surface controlled.^{7,9-11} Since the b value is the sum of faradaic response of diffusion controlled and capacitive effects, a closer examination from sweep rate voltammetry can be applied to quantify the capacitive effects (k_1v) and diffusion controlled behavior ($k_2v^{1/2}$) by following formula^{7,8,10,12}:

$$i = k_1v + k_2v^{1/2}$$

The k_1 and k_2 values can be determined by plotting $i/v^{1/2}$ vs $v^{1/2}$ (see Fig. S15d-f).

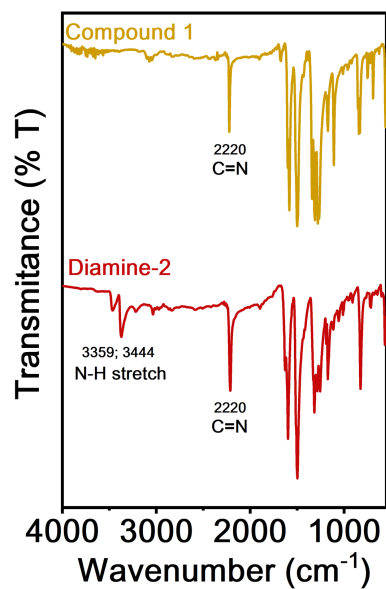


Fig. S1. The FTIR spectra of dinitro compound **1** and diamine monomer **Diamine-2**.

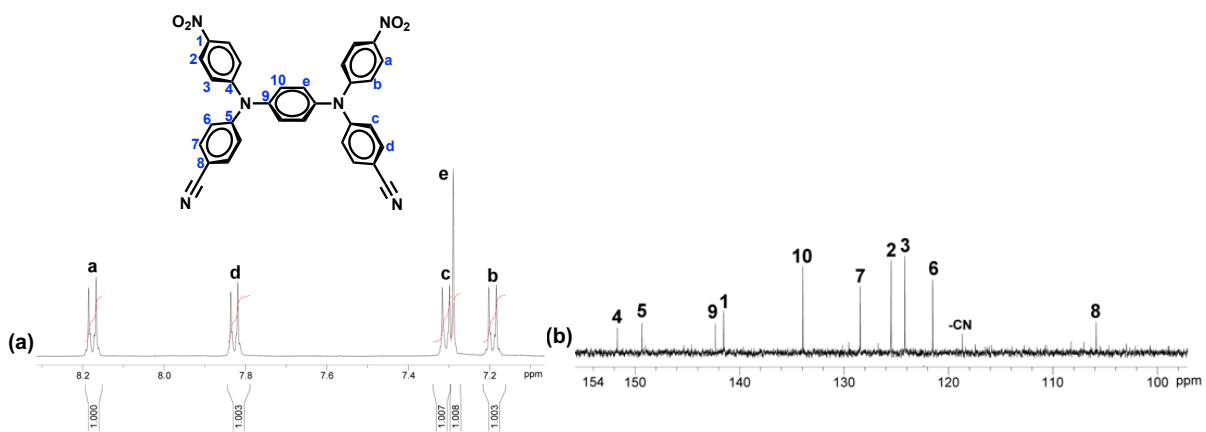


Fig. S2. (a) ^1H and (b) ^{13}C NMR spectra of dinitro compound **1** in $\text{DMSO}-d_6$.

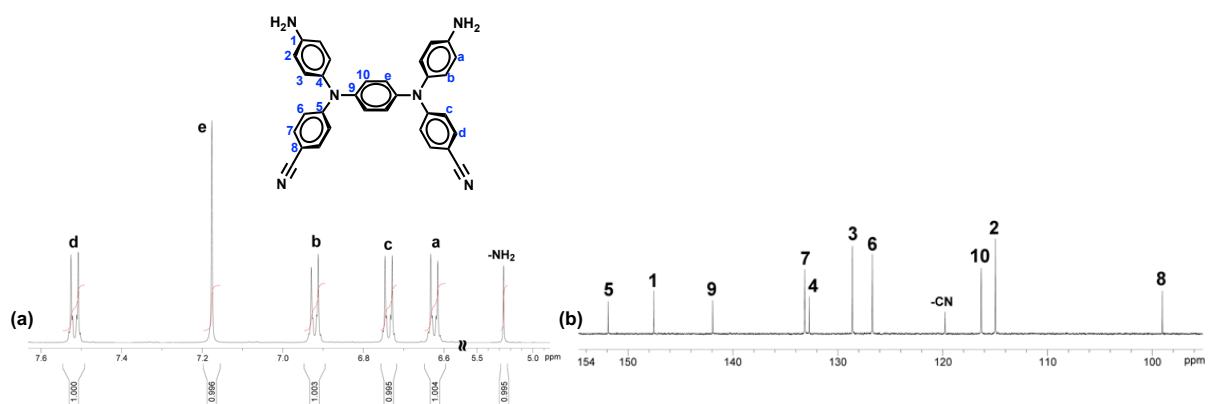


Fig. S3. (a) ^1H and (b) ^{13}C NMR spectra of diamine monomer **Diamine-2** in $\text{DMSO}-d_6$.

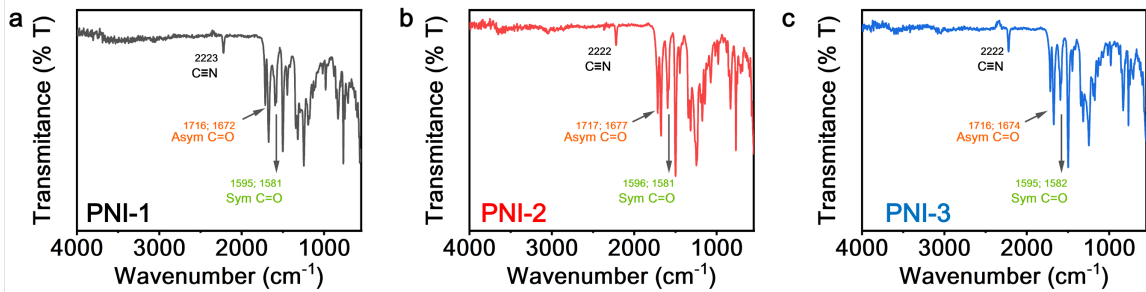


Fig. S4. FTIR spectra of TPA-PNIs. (a) PNI-1; (b) PNI-2; (c) PNI-3.

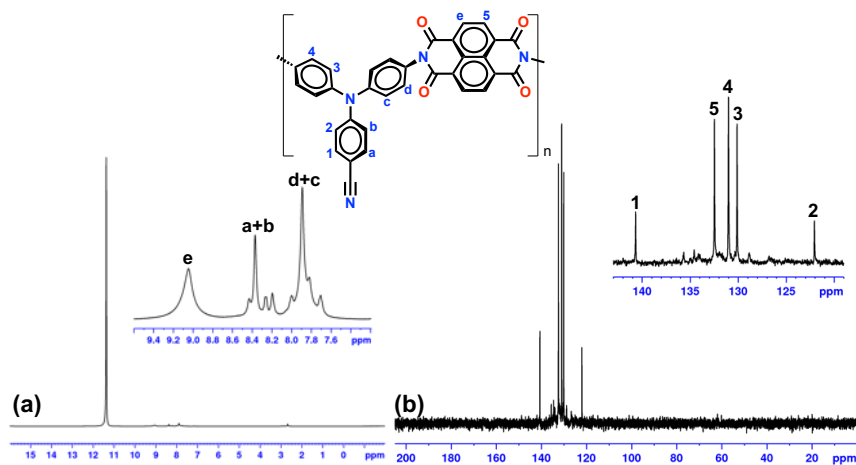


Fig. S5. (a) ^1H and (b) DEPT-135 NMR spectra of PNI-1 in D_2SO_4 .

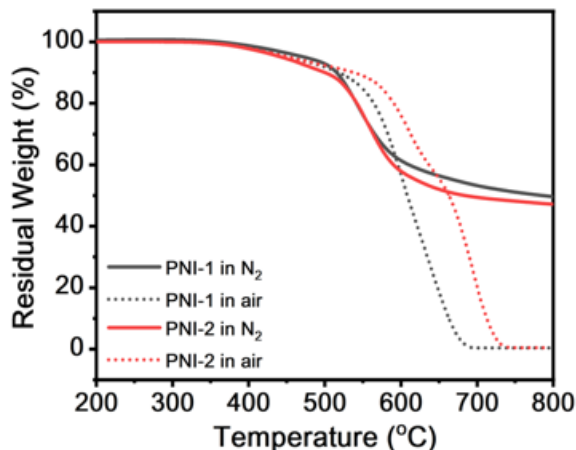


Fig. S6. TGA thermograms of PNIs in both air and nitrogen at a scan rate of 20 °C/min.

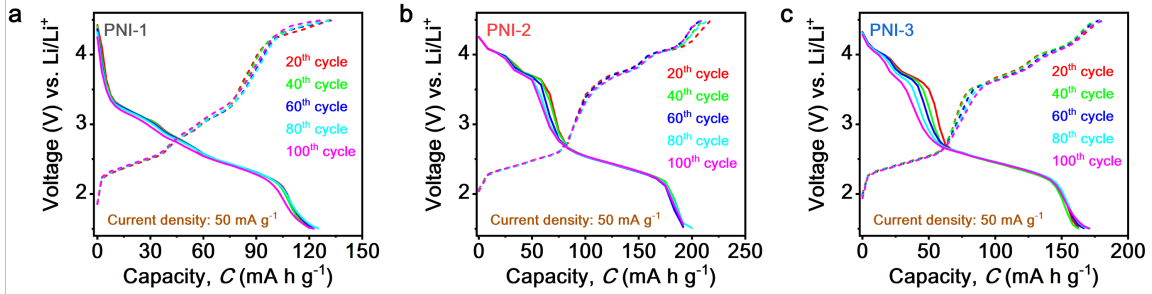


Fig. S7. Galvanostatic profile of TPA-PNI cathodes. (a) PNI-1; (b) PNI-2; (c) PNI-3.

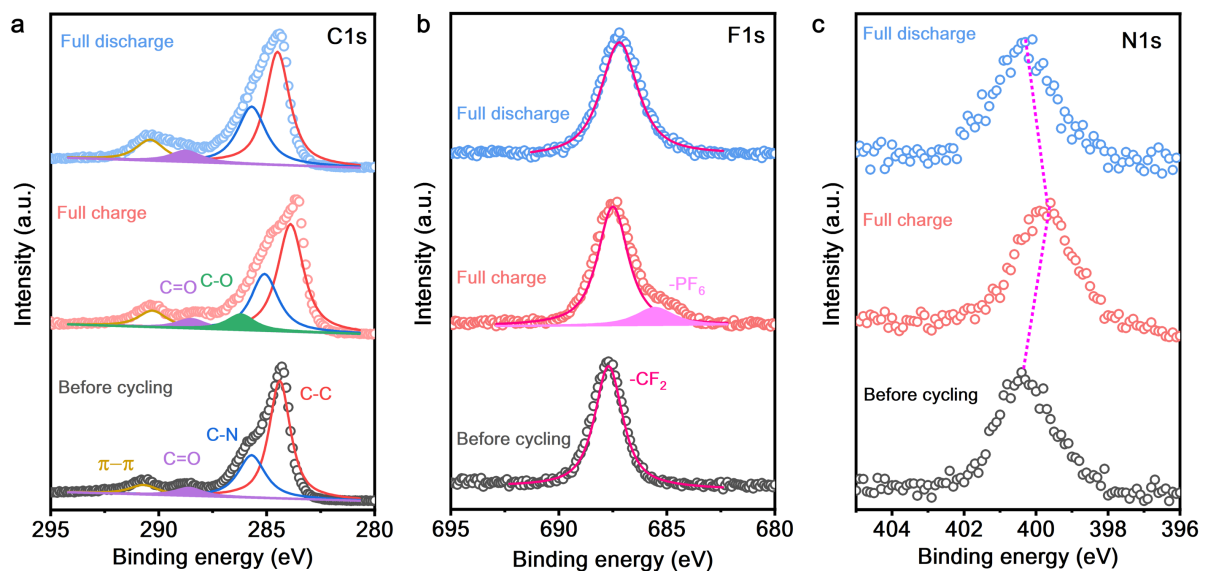


Fig. S8. Ex-situ XPS of PNI-2 cathode at different stages. (a) C1s; (b) F1s; (c) N1s.

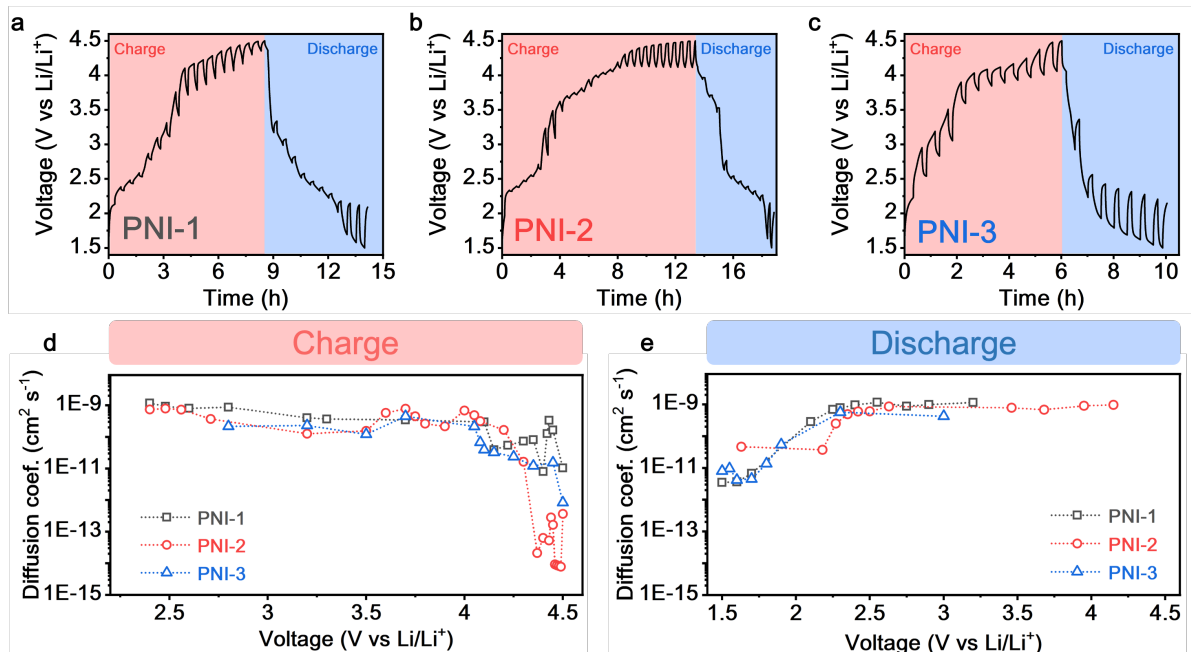


Fig. S9. The GITT profiles of (a) PNI-1; (b) PNI-2; (c) PNI-3. (d) and (e) are Li⁺ diffusion coefficient at charge and discharge stages, respectively.

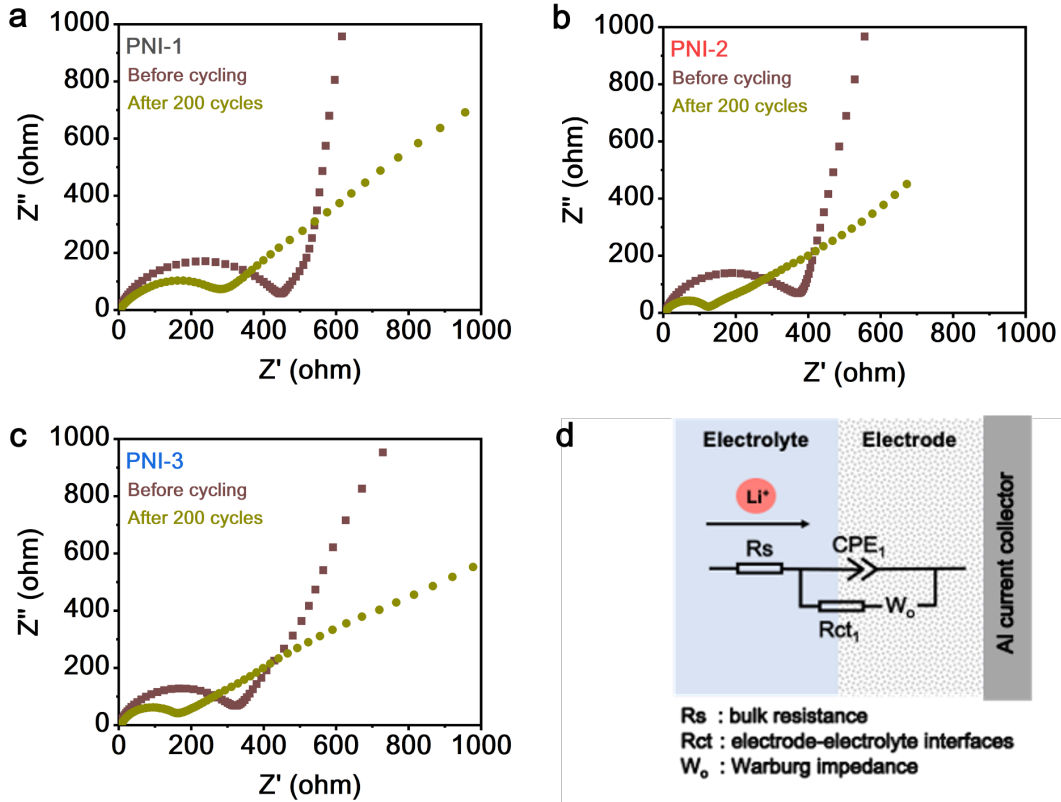


Fig. S10. Nyquist plots of TPA-PNI cathodes at different cycling intervals. (a) PNI-1; (b) PNI-2; (c) PNI-3; and (d) Equivalent circuit.

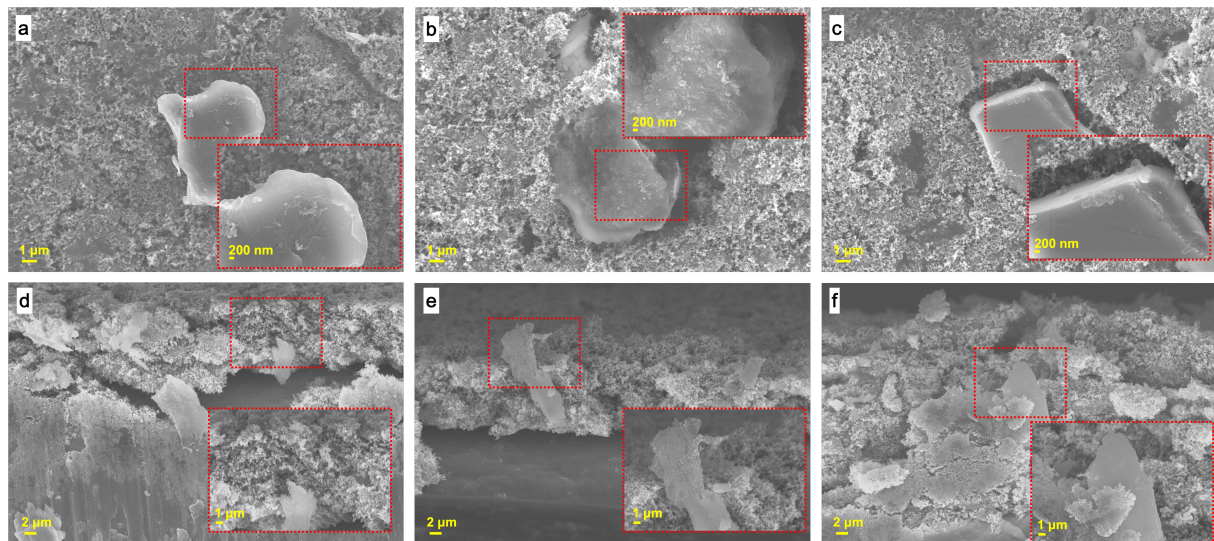


Fig. S11. The surface and cross-sectional FESEM images of PNIs before cycling. (a and d) PNI-1. (b and e) PNI-2. (c and f) PNI-3. The inset figures are the enlarged images from red-dashed square area.

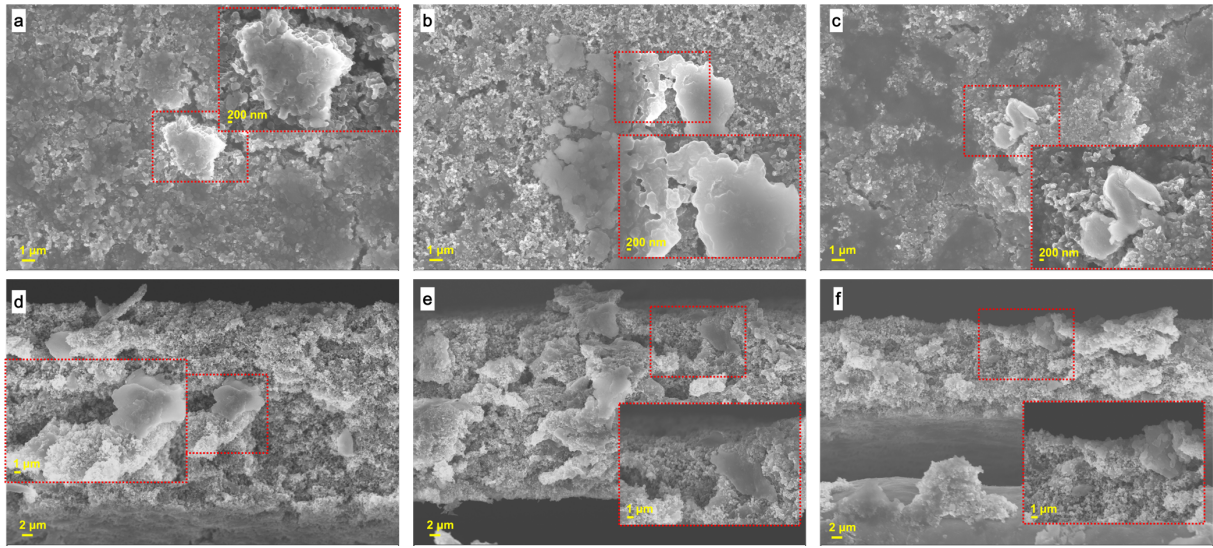


Fig. S12. The surface and cross-sectional FESEM images of PNIs after 5000 cycles. (a and d) PNI-1. (b and e) PNI-2. (c and f) PNI-3. The inset figures are the enlarged images from red-dashed square area.

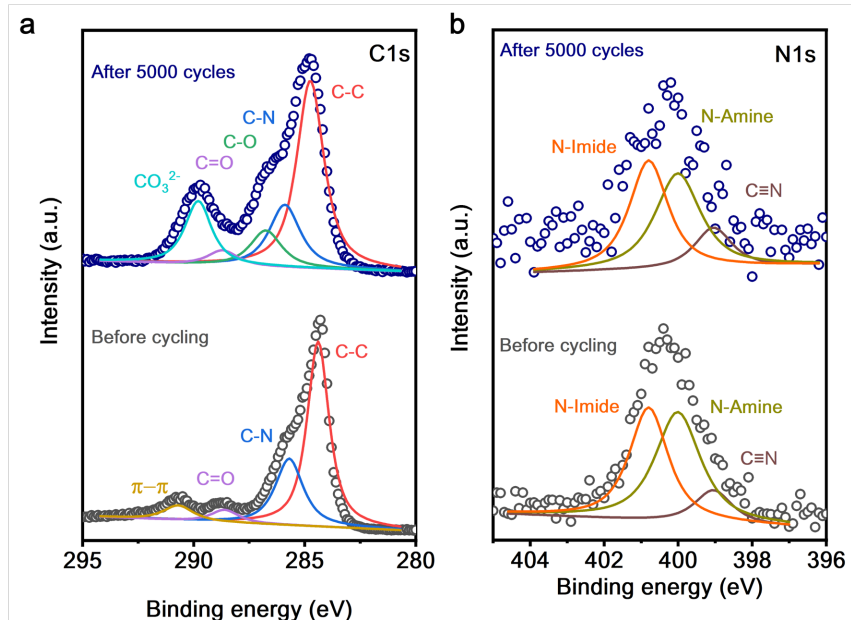


Fig. S13. *Ex-situ* XPS of PNI-2 at different cycling intervals. (a) and (b) are C1s and N1s spectra, respectively.

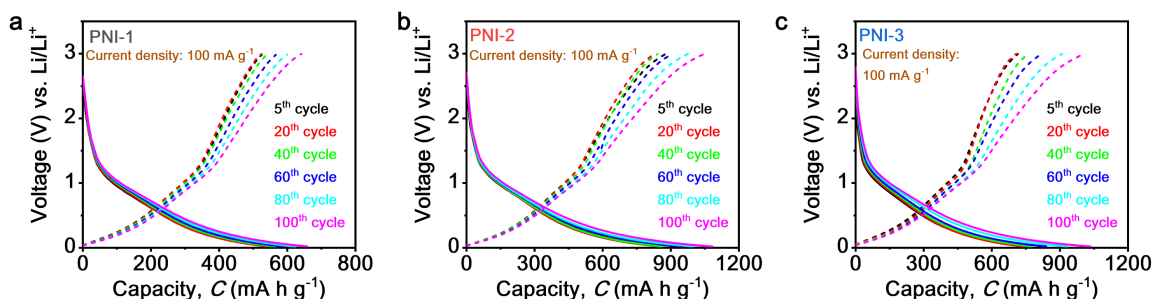


Fig. S14. Galvanostatic profile of TPA-PNI anodes. (a) PNI-1; (b) PNI-2; (c) PNI-3.

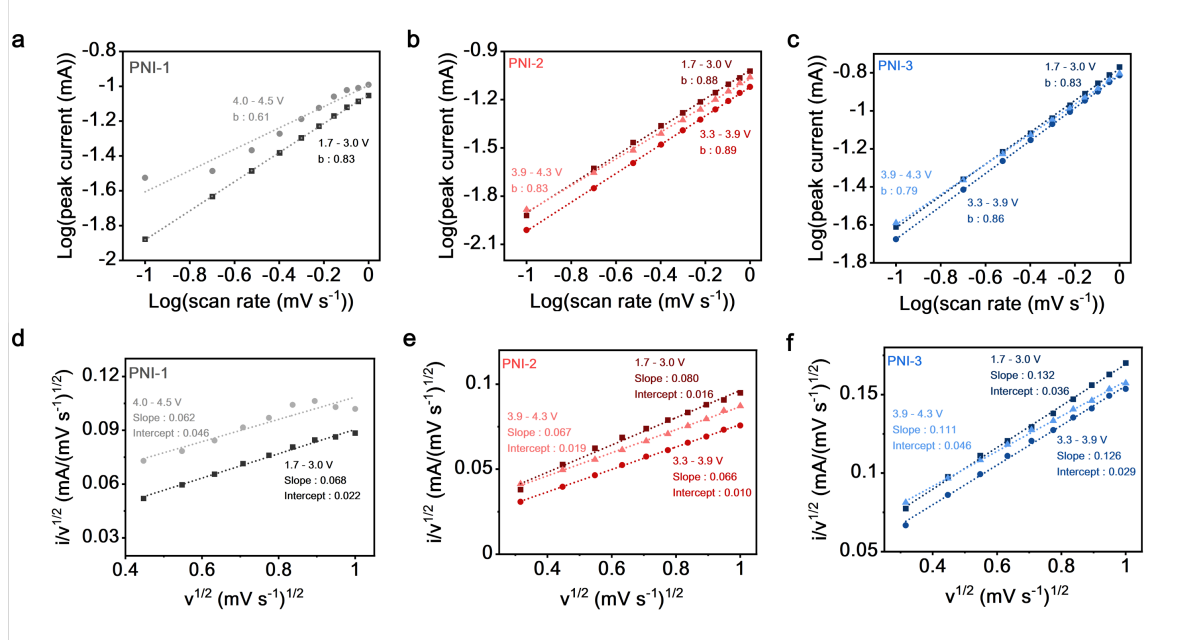


Fig. S15. (a – c) Log peak current vs log scan rate plot and (d – f) $v^{1/2}$ vs $i/v^{1/2}$ plot of TPA-PNIs.

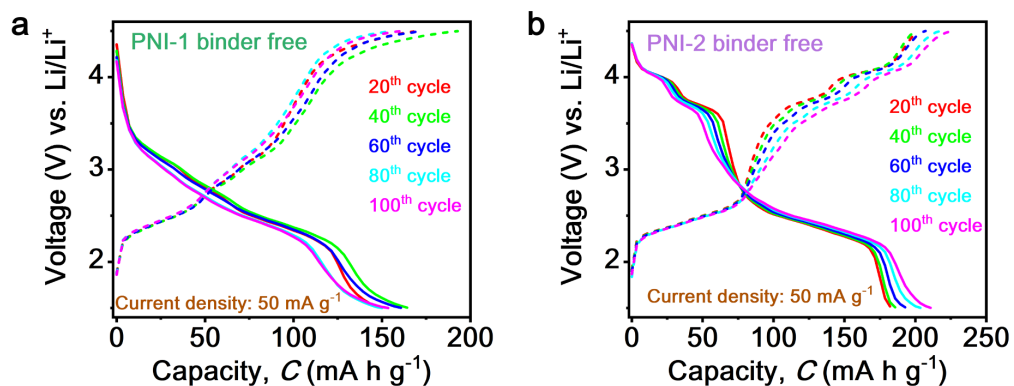


Fig. S16. Galvanostatic profile of binder-free TPA-PNI cathodes. (a) **PNI-1** (b) **PNI-2**.

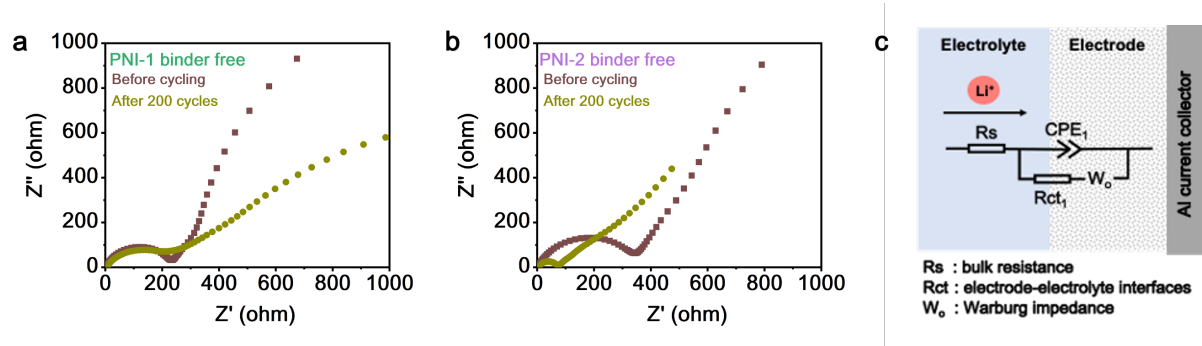
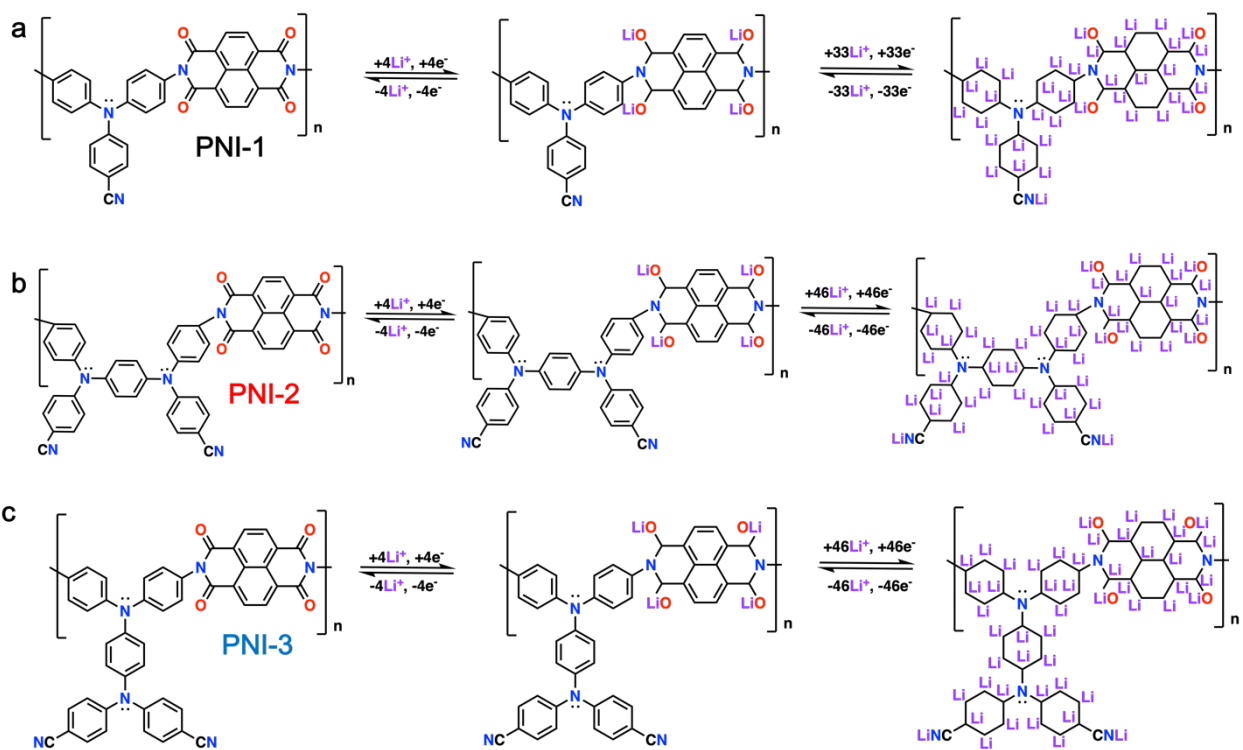


Fig. S17. Nyquist plots of binder-free TPA-PNI cathode at different cycling intervals. (a) **PNI-1**; (b) **PNI-2**; (c) Equivalent circuit.



Scheme S1. Schematic reaction mechanism of TPA-PNI anodes.

Table S1. Inherent viscosity^a and solubility behavior of PNIs

Code	η_{inh} (dL/g)	Solubility in various Solvent ^b					
		NMP	DMAc	DMF	<i>m</i> -Cresol	THF	CHCl ₃
PNI-1	0.75	+ −	−	−	++	−	−
PNI-2	0.45	+ −	+ −	−	++	−	−
PNI-3	0.38	+ −	+ −	−	++	−	−

^a Measured at a polymer concentration of 0.5 g/dL in *m*-cresol at 30 °C.

^b The solubility was determined with a 10 mg sample in 1 mL of a solvent. ++, soluble at room temperature; +, soluble on heating; + −, partially soluble or swelling; −, insoluble even on heating.

Table S2. Fitted EIS data TPA-PNI cathodes at different cycling interval.

Active material	Stages	R_s (Ω)	R_{ct} (Ω)	D_{Li} ($\text{cm}^2 \text{s}^{-1}$)
PNI-1	Before cycling	4.83	375.90	2.98×10^{-15}
	After 200 cycles	5.01	191.80	6.19×10^{-14}
PNI-2	Before cycling	6.55	336.50	5.59×10^{-15}
	After 200 cycles	7.02	88.29	1.96×10^{-12}
PNI-3	Before cycling	4.23	276.60	5.25×10^{-15}
	After 200 cycles	7.08	105.64	6.96×10^{-13}

Table S3. Fitted EIS data binder free TPA-PNI cathodes at different cycling interval.

Active material	Stages	R_s (Ω)	R_{ct} (Ω)	D_{Li} ($\text{cm}^2 \text{ s}^{-1}$)
Binder-free PNI-1	Before cycling	5.72	222.03	2.68×10^{-14}
	After 200 cycles	6.78	119.00	1.20×10^{-13}
Binder-free PNI-2	Before cycling	5.29	313.96	2.56×10^{-14}
	After 200 cycles	7.46	57.64	3.49×10^{-12}

Table S4. Summary of polymer based cathode for lithium-ion battery.

Polymer Type	Polymer Name	Open Voltage (V vs Li/Li ⁺)	Current density (mA g ⁻¹)	Spesific Capacity (mAh g ⁻¹)	Ref
Polyimide	Benzoquinone-based Polyimide (PMAQ)	1.5 – 3.5	0.2 C (1C = 427 mA g ⁻¹)	118 (100 cycles)	13
	Naphthalene-based Polyimide with urea (NOP)			153 (60 cycles)	
	Naphthalene-based Polyimide with ethylenediamine (NEP)	1.5 – 3.5	50	121 (60 cycles)	14
	Graphene-PI composite	1.5 – 3.5	50	200 (100 cycles)	15
	pPI	1.5 – 3.5	500	40 (1000 cycles) 80 (1000 cycles)	16
	mpi				
	3D Graphene network polyimide	1.5 – 3.5	0.5 C (1C = 221 mA g ⁻¹)	101 (1000 cycles)	17
	PDI-Bz	1.5 – 3.5	25	60 (50 cycles) 110 (50 cycles)	18
	PDI-Ur				
Polyquinone	PDDP-NI	1.0 – 4.2	0.1 C	150 (70cycles)	19
	TPA-NTCPI	1.5 – 3.5	100	150 (100cycles)	20
	PQANP-3	1.5 – 3.5	200	108.1 (5000 cycles)	21
	PAQS2	1.5 – 3.5	50	121 (100 cycles)	22
	PAQS	1.0 – 3.0	100	146 (100 cycles)	23
	PHBQS	1.5 – 3.7	50	160 (340 cycles)	24
	PDPA-AQ	1.5 – 4.5	0.1 C	100 (100 cycles)	25
	PTPA-PO	2.0 – 4.2	20	121 (100cycles) 88.7 (100 cycles)	26
Polytriphenylamine	PTPA				
	PTPA-PO/CNT	2.0 – 4.2	20	128 (100cycles)	27
	PHTPA	2.0 – 4.2	20C (1C = 60 mAg ⁻¹)	60 (5000 cycles)	28
	PTTAB	2.5 – 4.2	20	87 (50 cycles)	29

Polymer Type	Polymer Name	Open Voltage (V vs Li/Li ⁺)	Current density (mA g ⁻¹)	Spesific Capacity (mAh g ⁻¹)	Ref
TPA-PNIs	PNI-1	1.5 – 4.5	50	125 (100 cycles)	This work
			2000	75 (5000 cycles)	
	Binder free PNI-1	1.5 – 4.5	50	160 (100 cycles)	
			2000	75 (5000 cycles)	
	PNI-2	1.5 – 4.5	50	195 (100 cycles)	
			2000	130 (5000 cycles)	
	Binder free PNI-2	1.5 – 4.5	50	202 (100 cycles)	
			2000	115 (5000 cycles)	
	PNI-3	1.5 – 4.5	50	170 (100 cycles)	
			2000	110 (5000 cycles)	

Table S5. Summary of polymer-based LiB anodes.

Polymer type	Polymer name	Open Voltage (V vs. Li/Li ⁺)	Current Density (mA g ⁻¹)	Specific Capacity (mA h g ⁻¹)	Ref.
Conjugated pores polymer	Azo-BT (benzothiadiazole)			725 (500 cycles)	
	Azo-Py (pyrene)	0.005 – 3.0	50	619 (500 cycles)	30
	Azo-Bz (Benzene)			503 (500 cycles)	
	Polymer 4,7-dicarbazyl-[2,1,3]-benzothiadiazole (PDCzBT)	0.0 – 3.0	100 200	404 (100 cycles) 312 (400 cycles)	31
Polyanhydride	Polydiaminophenylsulfone-Triazine	0.0 – 3.0	100 1000	565 (100 cycles) 375 (100 cycles)	32
	SNW-1/CNTs	0.01 – 3.0	500	203 (1000 cycles)	33
	Poly(dihydroanthracene succinic anhydride)	0.2 – 3.0	50	1100 (1000 cycles)	34
Polyazaacene	Poly(1,6-dihydropyrazino[2,3g]quinoxaline-2,3,8-triyl-7-(2H)-ylidene-7,8-dimethylidene)	0.0 – 3.0	100	1550 (100 cycles)	35
Polybenzimidazole	MPBI-550	0.1 – 3.0	1000	700 (500 cycles)	36
Polystyrene	Hyper-crosslinked polystyrene (HPS)	0.0 – 3.0	200 2000	356 (100 cycles) 222 (1000 cycles)	37
Polythiophene	P(C-TDPP-TA)			357 (500 cycles)	
	P(F-TDPP-TA)			298 (500 cycles)	
	P(C-TDPP-H)	0.01 – 3.0	100	327 (500 cycles)	38
	P(F-TDPP-H)			278 (500 cycles)	
Polythiophene	DBD-CMP-1			315 (300 cycles)	
	DBD-CMP-2	0.005 – 3.0	100	595 (300 cycles)	39
Polythiophene	Poly(thiophene) (PT)			90 (1000 cycles)	
	Poly(3,3'-bithiophene) (P33DT)	0.0 – 3.0	500	663 (1000 cycles)	40
Polythiophene	PTp-COOH	0.01 – 3.0	500	147 (1000 cycles)	41
	Polytetra(2-thienyl)ethylene (PTTE)	0.005 – 3.0	500	585 (100 cycles)	42
	Poly-Triazine-Thiophene (PTT)-1			495 (300 cycles)	
Polythiophene	Poly-Triazine-Thiophene (PTT)-2	0.01 – 3.0	100	671 (300 cycles)	43

Polymer type	Polymer name	Open Voltage (V vs. Li/Li ⁺)	Current Density (mA g ⁻¹)	Specific Capacity (mA h g ⁻¹)	Ref.
Polyimide	Poly-Triazine-Thiophene (PTT)-3			707 (300 cycles)	
	Poly-Triazine-Thiophene (PTT)-4			772 (300 cycles)	
	P3-AQT	0.0 – 3.5	50	380 (100 cycles)	
			100	400 (100 cycles)	44
			500	400 (100 cycles)	
			1000	505 (100 cycles)	
	PMAQ	0.01 – 3.0	500	465 (150 cycles)	45
	PI	0.001 – 3.0	100	578 (50 cycles)	46
	PMTA	0.001 – 3.0	100	698 (50 cycles)	47
	Poly(imine-anthraquinone) (PIAQ)	0.01 – 3.5	200	1097 (100 cycles)	48
			1000	486 (1000 cycles)	
Polyquinone	Poly(benzobisimidazobenzophenanthroline) (BBL)	0.0 – 3.0	50	619 (100cycles)	49
	TPA-PMPI	0.02 – 3.0	100	1600 (100 cycles)	20
	N-CPIMs	0.0 – 3.0	10	500 (5 cycles)	50
	Polyanthraquinone-Triazine	0.01 – 3.0	200	1770 (400 cycles)	51
			1000	760 (400 cycles)	
TPA-PNIs	PNI-1		100	620 (100 cycles)	
			5000	490 (2000 cycles)	
	PNI-2	0.02 – 3.0	100	1092 (100 cycles)	This Work
			5000	500 (2000 cycles)	
	PNI-3		100	1042 (100 cycles)	
			5000	980 (2000 cycles)	

References:

1. T. Q. Nguyen and C. Breitkopf, *J. Electrochem. Soc.*, 2018, **165**, E826-E831.
2. T. Osaka, T. Momma, D. Mukoyama and H. Nara, *J. Power Sources*, 2012, **205**, 483-486.
3. H.-M. Cho, W.-S. Choi, J.-Y. Go, S.-E. Bae and H.-C. Shin, *J. Power Sources*, 2012, **198**, 273-280.
4. S. Rodrigues, N. Munichandraiah and A. K. Shukla, *J. Solid State Electrochem.*, 1999, **3**, 397-405.
5. E. Barsoukov and J. R. Macdonald, *Impedance Spectroscopy: Theory, Experiment, and Applications*, Wiley, 2018.
6. A. J. Bard and L. R. Faulkner, *Electrochemical Methods: Fundamentals and Applications, 2nd Edition*, Wiley Textbooks, 2000.
7. J. Wang, J. Polleux, J. Lim and B. Dunn, *J. Phys. Chem. C*, 2007, **111**, 14925-14931.
8. F.-F. Li, J.-F. Gao, Z.-H. He and L.-B. Kong, *ACS Appl. Energy Mater.*, 2020, **3**, 5448-5461.
9. V. Augustyn, J. Come, M. A. Lowe, J. W. Kim, P.-L. Taberna, S. H. Tolbert, H. D. Abruna, P. Simon and B. Dunn, *Nat. Mater.*, 2013, **12**, 518-522.
10. F. Yu, Z. Liu, R. Zhou, D. Tan, H. Wang and F. Wang, *Mater. Horizons*, 2018, **5**, 529-535.
11. H. Lindström, S. Södergren, A. Solbrand, H. Rensmo, J. Hjelm, A. Hagfeldt and S.-E. Lindquist, *J. Phys. Chem. B*, 1997, **101**, 7717-7722.
12. T. C. Liu, *J. Electrochem. Soc.*, 1998, **145**, 1882.
13. Z. Ba, Z. Wang, M. Luo, H.-b. Li, Y. Li, T. Huang, J. Dong, Q. Zhang and X. Zhao, *ACS Appl. Mater. Interfaces*, 2020, **12**, 807-817.
14. C. Chen, X. Zhao, H.-B. Li, F. Gan, J. Zhang, J. Dong and Q. Zhang, *Electrochim. Acta*, 2017, **229**, 387-395.
15. Y. Huang, K. Li, J. Liu, X. Zhong, X. Duan, I. Shakir and Y. Xu, *J. Mater. Chem. A*, 2017, **5**, 2710-2716.
16. R. R. Kapaev, A. G. Scherbakov, A. F. Shestakov, K. J. Stevenson and P. A. Troshin, *ACS Appl. Energy Mater.*, 2021, **4**, 4465-4472.
17. Y. Meng, H. Wu, Y. Zhang and Z. Wei, *J. Mater. Chem. A*, 2014, **2**, 10842-10846.
18. M. Ruby Raj, R. V. Mangalaraja, D. Contreras, K. Varaprasad, M. V. Reddy and S. Adams, *ACS Appl. Energy Mater.*, 2020, **3**, 240-252.
19. C. Zhang, S. Chen, G. Zhou, Q. Hou, S. Luo, Y. Wang and G. Shi, *J. Electrochem. Soc.*, 2021, **168**, 050548.
20. K. B. Labasan, H.-J. Lin, F. Baskoro, J. J. H. Togonon, H. Q. Wong, C.-W. Chang, S. D. Arco and H.-J. Yen, *ACS Appl. Mater. Interfaces*, 2021, **13**, 17467-17477.
21. Y. Shi, J. Yang, J. Yang, Z. Wang, Z. Chen and Y. Xu, *Adv. Funct. Mater.*, 2022, **32**, 2111307.
22. G. Ding, L. Zhu, Q. Han, L. Xie, X. Yang, L. Chen, G. Wang and X. Cao, *Electrochim. Acta*, 2021, **394**, 139116.
23. Y. Hu, Y. Gao, L. Fan, Y. Zhang, B. Wang, Z. Qin, J. Zhou and B. Lu, *Adv. Energy Mater.*, 2020, **10**, 2002780.
24. J. Bitenc, K. Pirnat, G. Mali, B. Novosel, A. Randon Vitanova and R. Dominko, *Electrochim. Commun.*, 2016, **69**, 1-5.
25. W. Huang, T. Jia, G. Zhou, S. Chen, Q. Hou, Y. Wang, S. Luo, G. Shi and B. Xu, *Electrochim. Acta*, 2018, **283**, 1284-1290.
26. J. Xiong, Z. Wei, T. Xu, Y. Zhang, C. Xiong and L. Dong, *Polymer*, 2017, **130**, 135-142.
27. T. Xu, J. Xiong, X. Du, Y. Zhang, S. Song, C. Xiong and L. Dong, *J. Phys. Chem. C*, 2018, **122**, 20057-20063.
28. K. Yamamoto, D. Suemasa, K. Masuda, K. Aita and T. Endo, *ACS Appl. Mater. Interfaces*, 2018, **10**, 6346-6353.

29. Z. Chen, W. Li, Y. Dai, N. Xu, C. Su, J. Liu and C. Zhang, *Electrochim. Acta*, 2018, **286**, 187-194.
30. W. Ma, C. Zhang, X. Gao, C. Shu, C. Yan, F. Wang, Y. Chen, J. H. Zeng and J.-X. Jiang, *J. Power Sources*, 2020, **453**, 227868.
31. S. Zhang, W. Huang, P. Hu, C. Huang, C. Shang, C. Zhang, R. Yang and G. Cui, *J. Mater. Chem. A*, 2015, **3**, 1896-1901.
32. Q. Ma, J. Zheng, H. Kang, L. Zhang, Q. Zhang, H. Li, R. Wang, T. Zhou, Q. Chen, A. Liu, H. Li and C. Zhang, *ACS Appl. Mater. Interfaces*, 2021, **13**, 43002-43010.
33. S.-X. Xu, W. Xu, L.-J. Kong and Y.-H. Zhang, *SN Appl. Sci.*, 2020, **2**, 199.
34. D. Mukherjee, G. Gowda Y. K, H. Makri Nimbegondi Kotresh and S. Sampath, *ACS Appl. Mater. Interfaces*, 2017, **9**, 19446-19454.
35. J. Wu, X. Rui, G. Long, W. Chen, Q. Yan and Q. Zhang, *Angew. Chem. Int. Ed.*, 2015, **54**, 7354-7358.
36. S. Ren, L. Meng, C. Ma, Y. Yu, Y. Lou, D. Zhang, Y. Han, Z. Shi and S. Feng, *Chem. Eng. J.*, 2021, **405**, 126621.
37. Z. Li, W. Zhong, A. Cheng, Z. Li, L. Li and H. Zhang, *Electrochim. Acta*, 2018, **281**, 162-169.
38. Z. Xu, S. Hou, Z. Zhu, P. Zhou, L. Xue, H. Lin, J. Zhou and S. Zhuo, *Nanoscale*, 2021, **13**, 2673-2684.
39. T. Yang, C. Zhang, W. Ma, X. Gao, C. Yan, F. Wang and J.-X. Jiang, *Solid State Ionics*, 2020, **347**, 115247.
40. C. Zhang, Y. He, P. Mu, X. Wang, Q. He, Y. Chen, J. Zeng, F. Wang, Y. Xu and J.-X. Jiang, *Adv. Funct. Mater.*, 2018, **28**, 1705432.
41. H. Numazawa, K. Sato, H. Imai and Y. Oaki, *NPG Asia Mater.*, 2018, **10**, 397-405.
42. X. Wang, C. Zhang, Y. Xu, Q. He, P. Mu, Y. Chen, J. Zeng, F. Wang and J.-X. Jiang, *Macromol. Chem. Phys.*, 2018, **219**, 1700524.
43. X. Xue, J. Luo, L. Kong, J. Zhao, Y. Zhang, H. Du, S. Chen and Y. Xie, *RSC Adv.*, 2021, **11**, 10688-10698.
44. C. Zhang, S. Chen, G. Zhou, Q. Hou, S. Luo, Y. Wang, G. Shi and R. Zeng, *J. Electroanal. Chem.*, 2021, **895**, 115495.
45. Z. Ba, Z. Wang, Y. Zhou, H. Li, J. Dong, Q. Zhang and X. Zhao, *ACS Appl. Energy Mater.*, 2021, **4**, 13161-13171.
46. J. He, Y. Liao, Q. Hu, Z. Zeng, L. Yi, Y. Wang, H. Lu and M. Pan, *Ionics*, 2020, **26**, 3343-3350.
47. J. He, Y. Liao, Q. Hu, Z. Zeng, L. Yi, Y. Wang, H. Lu and M. Pan, *J. Power Sources*, 2020, **451**, 227792.
48. Z. Man, P. Li, D. Zhou, R. Zang, S. Wang, P. Li, S. Liu, X. Li, Y. Wu, X. Liang and G. Wang, *J. Mater. Chem. A*, 2019, **7**, 2368-2375.
49. J. Wu, X. Rui, C. Wang, W.-B. Pei, R. Lau, Q. Yan and Q. Zhang, *Adv. Energy Mater.*, 2015, **5**, 1402189.
50. X. Han, P. Han, J. Yao, S. Zhang, X. Cao, J. Xiong, J. Zhang and G. Cui, *Electrochim. Acta*, 2016, **196**, 603-610.
51. H. Kang, H. Liu, C. Li, L. Sun, C. Zhang, H. Gao, J. Yin, B. Yang, Y. You, K.-C. Jiang, H. Long and S. Xin, *ACS Appl. Mater. Interfaces*, 2018, **10**, 37023-37030.